https://doi.org/10.1016/j.asr.2017.05.038

A study of multi-GNSS ionospheric scintillation and cycle-slip over Hong Kong region for moderate solar flux conditions

Xiaomin Luo[a,b], Zhizhao Liu[b,*], Yidong Lou[a,*], Shengfeng Gu[a], Biyan Chen[b]

[a] *GNSS Research Center, Wuhan University, Luoyu Road 129, Wuhan 430079, Hubei, China*

[b] *Department of Land Surveying and Geo-Informatics, The Hong Kong Polytechnic University, 11 Yuk Choi Road, Kowloon, Hong Kong*

Abstract

This study presents the characteristics of Multiple Global Navigation Satellite System (Multi-GNSS) ionospheric scintillation and cycle-slip occurrence through the analysis of Multi-GNSS data collected by a newly installed receiver located at Sha Tin of Hong Kong from 6 October 2015 to 31 December 2016. This period of time was under a moderate solar activity condition with average sunspot number and $F10.7$ as 44 and 92, respectively. Considering the frequent occurrence of loss of lock in satellites measurements in the presence of ionospheric scintillation, a rate of geometry-free (ROGF) combination is proposed to take the time gap size between two data arcs into account in the cycle-slip detection. The results show that most ionospheric scintillation events and cycle-slips are observed from 20:00 LT to 0:00 LT. Under the strong scintillation ($S_4 >$ 0.6) conditions, it is found that the time series of wide-land (WL) ambiguity N_{WL} and $ROGF$ vary significantly and their range can reach more than 50 cycles and 0.1 m/s, respectively. However, the variations of the N_{WL} and $ROGF$ are generally small under weak scintillation ($0.2 < S_4 \leq 0.6$) or non-scintillation ($S_4 \leq 0.2$) conditions. A strong correlation of scintillation and cycle-slip occurrence is also verified by the daily and spatial statistics results. In addition, it is found that on average every 1000 strong scintillation events can result in 200, 124, and 171 cycle-slip occurrences in GPS, GLONASS, and BDS, respectively, whereas these values are 7, 12, and 12 per 1000 under weak scintillation conditions. This study suggests that cautions be taken when GNSS measurements are contaminated by the strong ionospheric scintillation in GNSS applications such as real-time kinematic (RTK) and precise point positioning (PPP).

Keywords: Multiple global navigation satellite system, Ionospheric scintillation, Cycle-slip, Low-latitude

1. Introduction

Ionosphere has a significant impact on satellite navigation, communications, and radar systems. As satellite radio signals propagate from space through the ionosphere to the ground, they would suffer various ionospheric effects such as phase fluctuations, amplitude fluctuations, group delay, absorption, scattering, and frequency shifts (Bernhardt et al., 2006; Chen et al., 2008). Ionospheric scintillation is a random fluctuation of amplitude and phase while radio signals pass through ionospheric plasma irregularities. Ionospheric scintillation can be classified into amplitude scintillation and phase scintillation (Crane, 1977), which are usually characterized by indexes S_4 and σ_φ, respectively (Van Dierendock et al., 1993). Scintillations frequently occur in the equatorial, low-latitude and polar region, especially during solar maximum (Li et al., 2010; Meggs et al., 2008; Moreno et al., 2011). Scintillations occurring in equatorial and low-latitude are mainly caused by equatorial F-region

* Corresponding author.

E-mail address: lszzliu@polyu.edu.hk (Z. Liu), ydlou@whu.edu.cn (Y. Lou).

irregularities, which encompass a wide range of scale sizes from several hundred kilometers to a few centimeters (Kil and Heelis, 1998). Scintillations occurring in polar region are mainly caused by steep ionospheric density gradients associated with auroral arc and cusp precipitation as well as polar cap patches (Prikryl et al., 2013; Weber et al., 1984). Strong amplitude and phase scintillations can be observed at equational and low-latitude regions (Jiao and Morton, 2015). In high-latitude regions, phase scintillations are more frequent and intense than amplitude ones (Jiao et al., 2013; Skone et al., 2008).

Ionospheric scintillation can degrade the data quality of many Earth observation systems such as GNSS, astronomical observations, and Doppler Orbit and Radio Positioning Integration by Satellite (DORIS) (Aquino et al., 2005; Bernhardt et al., 2006; Milan et al., 2005; Sreeja et al., 2011). To GNSS users, amplitude scintillation possibly leads to signal-to-noise-ratio (SNR) of GNSS signal level that drops below the receiver's phase lock loop (PLL), while phase scintillation can cause an apparent Doppler shift that sometimes exceeds the bandwidth of the receiver's PLL. Before reacquiring the signal, a delay in receiver would be generated. This phenomenon is called cycle-slip (Banville et al., 2010). One cycle of slip in GNSS carrier phase data can bring in a range error of ~ 20 cm to GPS L_1 measurements (Liu, 2011), which may result in an intolerable error to the GNSS positioning solution. In GNSS real-time kinematic (RTK) and precise point positioning (PPP) applications, positioning precision of decimeter and even centimeter depends on reliable and high quality carrier phase measurements that have no cycle-slips or have cycle-slips corrected (Ge et al., 2008; Grejner-Brzezinska et al., 2007). On the other hand, it is a big challenge to detect and especially correct cycle-slip occurring in ionospheric scintillation compared to the case without scintillation. Under scintillations, observational noise will become larger because of the fading of GNSS measurements. In addition, continuous cycle-slips can occur and last several minutes owing to intensive ionospheric scintillations. Therefore, investigating a suitable method of cycle-slip detection and analyzing the characteristics of cycle-slip occurrence in the presence of ionospheric scintillation are of significant value to both GNSS manufacturers and users.

Over the past years, the study of cycle-slip occurrence in the presence of ionospheric scintillation has been an interesting research area, in which there are two focuses in general, i.e. methods of cycle-slip detection and correction (Banville et al., 2010; Banville and Langley, 2013; Ji et al., 2013b) and characteristics of cycle-slip occurrence (Prikryl et al., 2014; Zhang et al., 2010). For the former research topic, Banville and Langley (2013) proposed a geometry-based approach to detect cycle-slip and applied the least-squares adjustment to determine their magnitude. This technique is effective in resolving the discontinuities of carrier-phase measurements caused by ionospheric irregularity. In order to mitigate code measurement noise in the presence of ionospheric scintillation, Ji et al. (2013b) used carrier-phase measurements to combine non-geometry-free and ionosphere-free quantities to detect and correct cycle-slip. However, the threshold of cycle-slip occurrence was not discussed in Ji et al. (2013b). In the study of the characteristics of cycle-slip occurrence, focusing on high-latitude region, Prikryl et al. (2010) reported numerous GPS cycle-slips and strong scintillation observed during solar minimum of 2008–2009, which were associated with auroral arc and polar cap patches. More recently, the characteristics of occurrence of phase scintillation and cycle-slip during high-speed solar wind streams and interplanetary coronal mass ejections are shown in Prikryl et al. (2014). It illustrates that phase scintillation and cycle-slip occur predominantly on the dayside in the cusp and in the nightside auroral oval. However, quantitative analysis of cycle-slips and scintillation events is not shown in the aforementioned two references. For low-latitude region, Zhang et al. (2010) investigated the features of GPS cycle-slip occurrences related to ionospheric irregularities. Based on GPS data collected at China low-latitude region, it is found that cycle-slips frequently occur in 19:00–22:00 local time (LT). Meanwhile, coincided with seasonal occurrence of ionospheric scintillation over the Asia-Pacific longitude sector, most cycle-slips have been detected in the equinox months. Zhang et al. (2010) shows the relationship between the number of cycle-slip occurrences and

ionospheric irregularities, which is expressed by the spread *F* (SF) data as well as Ap index. Nevertheless, different from scintillation indexes S_4 and σ_φ, the SF data or Ap index is unable to completely illustrate the real level of ionospheric scintillation (Jiao and Morton, 2015). Most recently, the aspect of scintillation enhancement and loss of phase lock (cycle-slip) conditions due to field-aligned (longitudinal) propagation for low-latitude region is discussed in de Oliveira Moraes et al. (2017).

Located in the geomagnetic equatorial region, GNSS receivers in Hong Kong area (geographic 22.3°N, 114.2°E) often experience strong scintillations (Chen et al., 2008; Ji et al., 2013a; Xu et al., 2012). Previous studies in Hong Kong showed that ionospheric disturbances were observed in more than one third time of year during the solar maximum of 2001 (Chen et al., 2008). In addition, the number of losses of lock for Leica CRS receiver can reach up to 500 per day in strong scintillations, while in quiet days it significantly decreases to 50 per day (Chen et al., 2008). Compared to previous studies, this work represents the first attempt to investigate the characteristics of ionospheric scintillation and cycle-slip occurrence using multi-GNSS (i.e., GPS, GLONASS, BDS, and Galileo) data collected at Sha Tin station in Hong Kong.

In the following sections, we first describe the data and method used to compute two scintillation indexes and cycle-slip detection. Then, the hourly, daily, spatial distribution of scintillation event and cycle-slip are analyzed. Finally, a conclusion is given at the end of this paper.

2. Data and methodology

In this study, we used a newly installed Septentrio PolaRxS-Pro GNSS receiver at Sha Tin (22°25′N, 114°12′E; geomagnetic: 12°40′N, 173°32′W) of Hong Kong. It is a multi-constellation and multi-frequency receiver, with an ability to track signals from GPS ($L_1/L_2/L_5$), GLONASS (G_1/G_2), BDS (B_1/B_2), and Galileo (E_1/E_{5a}). The information on Multi-GNSS signals and frequencies is included in

Table 1. The receiver outputs the binary files containing 50 Hz raw correlation and phase data. After converting the binary files into the ASCII ISMR files, the amplitude scintillation index S_4, phase scintillation index σ_φ, and ionospheric total electron contents (TEC) indexes can be obtained. The S_4 index is computed with an interval of 60 s, which is the standard deviation of the receiver power I normalized by its mean value (Briggs and Parkin, 1963):

$$S_4^2 = \frac{\langle I^2\rangle - \langle I\rangle^2}{\langle I\rangle^2} \quad (1)$$

The σ_φ index is also computed with an interval of 60 s, which is characterized by the standard deviation φ of the detrended raw carrier phase and can be calculated as (Van Dierendonck et al., 1993):

$$\sigma_\varphi^2 = \langle \varphi^2\rangle - \langle \varphi\rangle^2 \quad (2)$$

Table 1 The information of Multi-GNSS satellites signals

	GNSS system	$L_1/G_1/B_1/E_1$	$L_2/G_2/B_2/E_{5b}$	$L_5/-/B_3/E_{5a}$	$-/-/-/E_5$
Carrier frequency (MHZ)	GPS	1575.42	1227.60	1176.45	-
	GLONASS	1602 + k*0.5625	1246 + k*0.4375	-	-
	BDS	1561.10	1207.14	1268.52	-
	Galileo	1575.42	1207.14	1176.45	1191.795
Wavelength (cm)	GPS	19.0	24.4	25.5	-
	GLONASS	18.7–18.8	24.0–24.1	-	-
	BDS	19.2	24.8	23.6	-
	Galileo	19.0	24.8	25.5	25.2
Modulation	GPS	BPSK	BPSK	BPSK	-
	GLONASS	BPSK	BPSK	-	-

	BDS	QPSK	QPSK	QPSK	-
	Galileo	CBOC	AltBOC	AltBOC	AltBOC

Note: k = –7…+12 (https://www.glonass-iac.ru/en/GLONASS/)

In our experiment, the dataset containing a total of 363 days of observation at the Sha Tin station during the period from 6 October 2015 to 31 December 2016 is used. Details on the number of available days and the corresponding percentage are listed in Table 2. **Error! Reference source not found.** shows the variability of the sunspot number and solar flux index $F10.7$ over the past two solar cycles. These indexes are widely used to characterize the conditions of the solar activity (de Oliveira Moraes et al., 2012). The rightmost gray area in **Error! Reference source not found.** corresponds to the study period of this paper. For the period of analysis, the average sunspot number and $F10.7$ are 44 and 92, respectively. It should be mentioned that the averaged $F10.7$ value of 92 is a moderate solar flux condition and the period of analysis follows immediately the peak of current solar cycle. In the data processing, only GNSS satellite measurements with an elevation mask angle higher than 30° are taken into consideration in order to minimize potential multipath effects.

Table 2 Number of available days and its percentage for multi-GNSS data used in this study

Year	2015		2016	
Month	No. of days	%	No. of days	%
Jan	Not available		31	100
Feb			29	100
Mar			31	100
Apr			1	3.3
May			20	64.5
Jun			30	100
Jul			24	77.4
Aug			0	0
Sep			18	60
Oct	26	83.9	31	100
Nov	30	100	30	100
Dec	31	100	31	100
Total	87	23.8	276	75.4

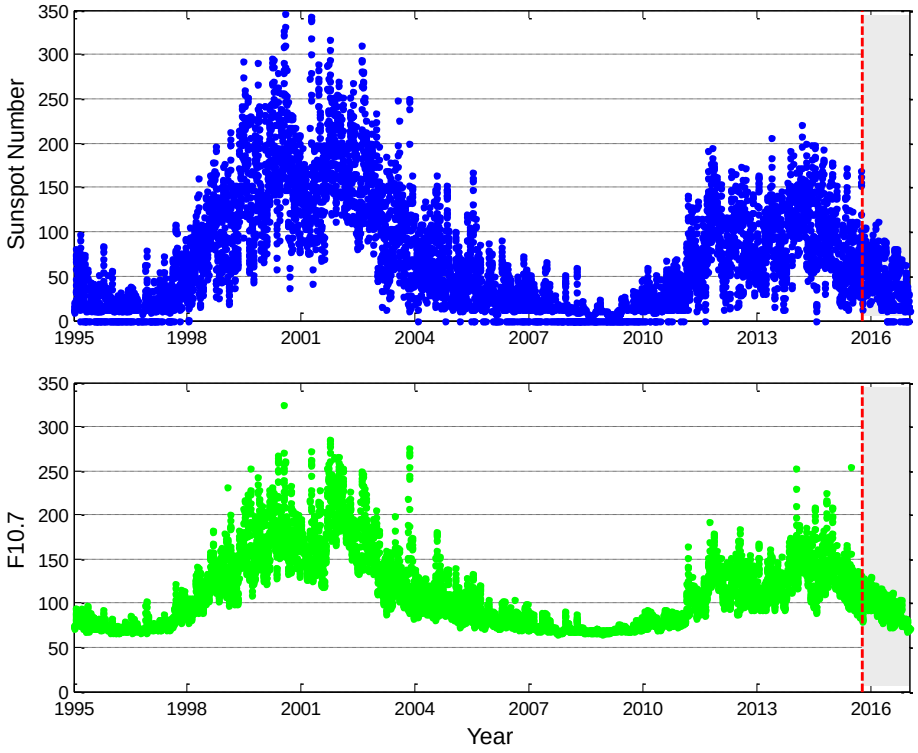

Fig. 1 The time series of sunspot number and solar flux index *F*10.7 in the past two solar cycles

A scintillation event is defined in this paper when this condition is satisfied: $S_4 > 0.2$ or $\sigma_\varphi > 15°$ (or 0.26 rad), which is commonly adopted as the threshold of scintillation occurrence in many past studies (Huang et al., 2014; Jiao et al., 2013; Jiao and Morton, 2015; Olwendo et al., 2016). If signals from more than one satellite transport the same ionospheric irregularity and the corresponding $S_4 > 0.2$ or $\sigma_\varphi > 15°$, each satellite scintillation is treated as a separate event.

The TurboEdit algorithm has been widely used to detect and repair cycle-slips on undifferenced, dual-frequency GNSS data. It is based on Melbourne-Wübbena WL and GF combinations (Blewitt, 1990), and two basic detection observables can be written as follows:

$$\Delta N_{WL} = \frac{\Delta L_{WL}}{\lambda_{WL}} = \Delta\varphi_1 - \Delta\varphi_2 - \frac{f_1 \cdot \Delta P_1 + f_2 \cdot \Delta P_2}{\lambda_{WL}(f_1 + f_2)} \tag{3}$$

$$\Delta\varphi_{GF} = \lambda_1 \cdot \Delta\varphi_1 - \lambda_2 \cdot \Delta\varphi_2 = \lambda_1 \cdot \Delta N_1 - \lambda_2 \cdot \Delta N_2 + (\gamma - 1)\Delta I \tag{4}$$

where Δ is the data arc difference operator; N_{WL} and φ_{GF} are the WL and GF combination observables, respectively; L_{WL} is the WL carrier phase measurement; $\lambda_{WL} = c/(f_1 - f_2)$; φ_1 and φ_2 are the carrier phases on L_1 and L_2 frequencies, respectively; P_1 and P_2 are the pesudoranges on L_1 and L_2 frequencies, respectively; f_1 and f_2 are carrier frequencies; N_1 and N_2 are the integer number of cycles on L_1 and L_2 frequencies, respectively; $\gamma = f_1^2/f_2^2$; I is the ionospheric range delay. In Eq. (3) and Eq. (4), the ΔN_{WL} and $\Delta\varphi_{GF}$ are computed with an interval of 30 s.

Under quiet ionospheric activity, the value of ionospheric delay I is stable in a short time interval (Blewitt, 1990). Therefore, the residual ionospheric delay ΔI usually can be ignored in the process of cycle-slip detection based on GF combination. On the contrary, during strong ionospheric activity, the change of ΔI is unpredictable, possibly reaching several decimeters sometimes (Banville et al., 2010). Thus the threshold of $\Delta\varphi_{GF}$ should be defined as a more flexible value (e.g. 0.5 m) to minimize the potential of misjudgment of cycle-slip detection (Zhang et al., 2014). Since the phenomenon of loss of lock frequently occurs in GPS L_1 and L_2 measurements in the presence of ionospheric scintillation, the strategy of cycle-slip detection should

further consider the size of the time gap between two data arcs (Chen et al., 2008). Considering the sampling interval of GPS measurement in cycle-slip detection and repair under different levels of ionospheric activity, Liu (2011) proposed a method based on TEC rate (TECR) to detect cycle-slip. Inspired by this, a rate of GF (ROGF) combination is proposed to detect cycle-slip in our study. The *ROGF* combination is defined as follows:

$$ROGF = \frac{\Delta\varphi_{GF}}{\triangle t} = \frac{\lambda_1 \cdot \triangle\varphi_1 - \lambda_2 \cdot \triangle\varphi_2}{\triangle t} \quad (5)$$

According to Zhang et al. (2014), the threshold values of ΔN_{WL} and $ROGF$ are defined 1.75 cycle and 0.02 m/s, respectively. It should be mentioned that outliers of GNSS measurements have been detected and removed before the operation of cycle-slip detection.

3. Results and analyses

3.1. Hourly distribution of scintillations and cycle-slips

Fig. 2 presents the time series of the S_4 and σ_φ for all the satellites from GPS, GLONASS, and BDS systems observed at Sha Tin station from 18:00 LT to 6:00 LT on DOY 321 in 2015 (17 November 2015). In Fig. 2, different colors in the right legend represent different satellites, and these colors are for all observed constellations. As an example, the S_4 and σ_φ information of the three satellite systems can be clearly seen during the twelve hours of DOY 321. From Fig. 2, we can notice that the time series of S_4 fluctuate significantly during 20:00 LT to 0:00 LT for GPS, GLONASS, and BDS, whereas most of the S_4 of other times are smaller than 0.2. The satellites with S_4 > 0.2 are G08, G14, G22, G23, G26, and G31 for GPS, R06, R07, and R10 for GLONASS, C01, C06, and C07 for BDS. The BDS satellite C01 is a geostationary earth orbit satellite and the C06 and C07 are inclined geosynchronous satellite orbit satellites. Similarly, the time series of σ_φ also fluctuate obviously during 20:00 LT to 0:00 LT as observed by the three systems. The satellites with σ_φ > 15° are G14, G22, and G26 for GPS, R06, R07, and R10 for GLONASS, C01, C06, and C07 for BDS. Fig. 2 shows that in low-latitudes phase scintillations are accompanied by amplitude scintillations but the amplitude scintillations could occur alone without the phase scintillations. This is consistent with the observation by Gwal et al. (2006) and Xu et al. (2012).

As we know, ionospheric scintillation leads to a higher possibility of cycle-slip occurrence. A distribution of cycle-slip detection indexes ΔN_{WL} and *ROGF* relative to scintillation indexes S_4 and σ_φ can directly show the frequency of cycle-slip occurrences at different scintillation levels. The time series of N_{WL} and *ROGF* in the presence of S_4 and σ_φ fluctuations, using satellite measurements of GPS G22, GLONASS R07, and BDS C01 observed on DOY 321 in 2015, are shown in Fig. 3. If no cycle-slip occurs, the variations of the N_{WL} and *ROGF* are small. In case of ionospheric scintillation, the variations would be different. As shown in Fig. 3, the time series of S_4 and σ_φ for GPS G22 fluctuate quickly during 21:07–21:57 LT and the maxima of S_4 and σ_φ are 1.01 and 78°, respectively. Due to the ionospheric scintillation effects, the values of WL ambiguity N_{WL} vary significantly during 21:07–21:57 LT and the range can reach more than 50 cycles. Similarly, the time series of *ROGF* fluctuate rapidly during 21:07–21:57 LT and the range reaches approximately 0.1 m/s. Similar phenomenon is also illustrated by the data from GLONASS R07 and BDS C01 in Fig. 3.

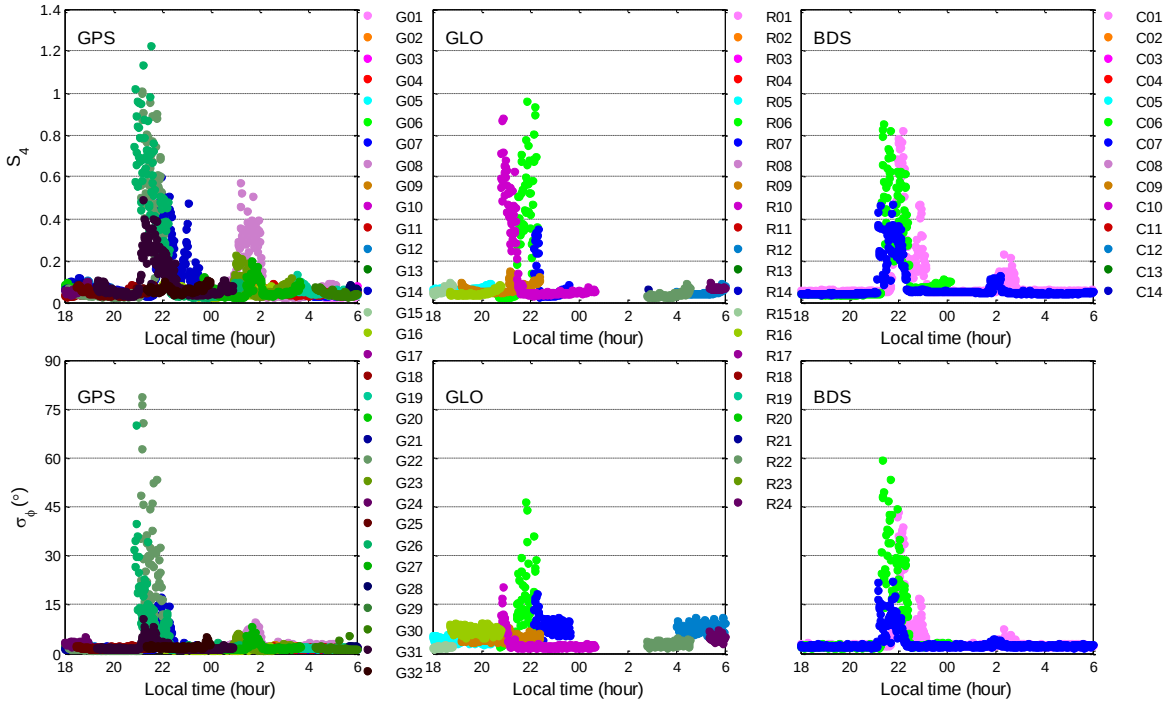

Fig. 2 The time series of S_4 and σ_φ for GPS, GLONASS and BDS satellites observed at Sha Tin station on DOY 321 in 2015. GPS, GLONASS, and BDS are referred to as G, R, and C, respectively

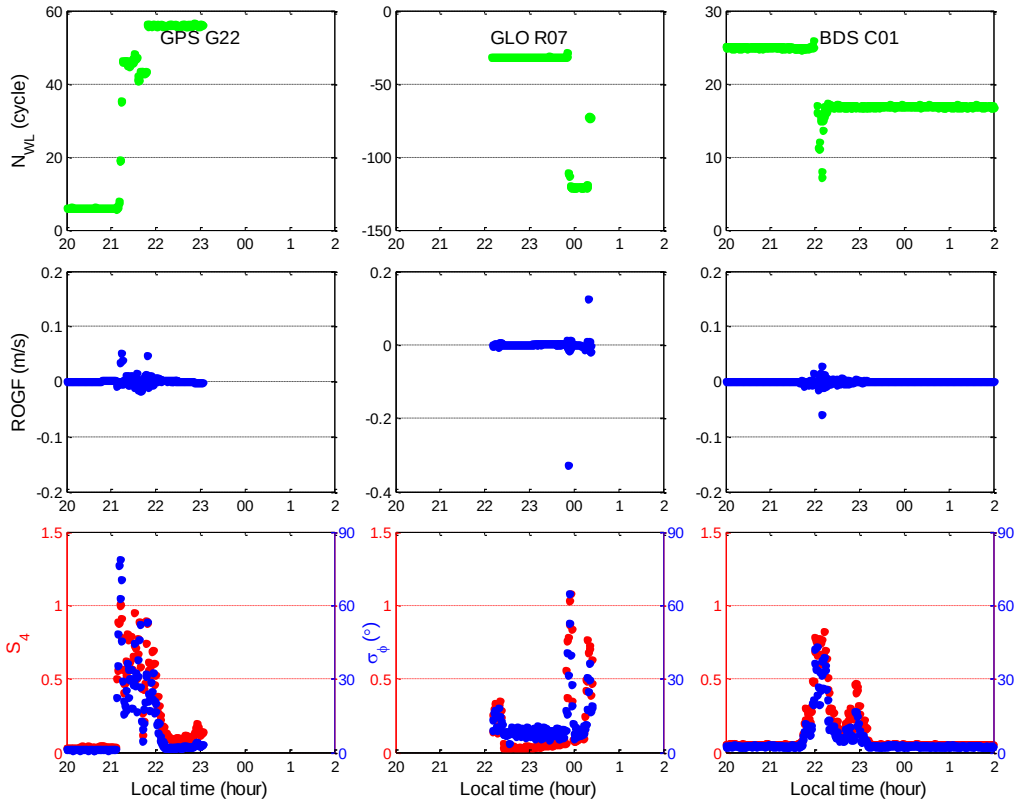

Fig. 3 The time series of N_{WL} and *ROGF* as well as S_4 and σ_φ for GPS G22, GLONASS R07, and BDS C01 observed at Sha Tin station on DOY 321 in 2015

The variation of ΔN_{WL} and *ROGF* (during cycle-slip occurrence) against S_4 and σ_φ for GPS,

GLONASS, and BDS satellites observed from 6 October 2015 to 31 December 2016 is shown in Fig. 4. The vertical dashed lines in left and right panels of Fig. 4 represent the threshold 0.2 and 15° for amplitude and phase scintillations, respectively. It should be mentioned that the cycle-slip events in the left and right panels have one-to-one correspondence. The left two panels of Fig. 4 show that the values of ΔN_{WL} (from −370 to 385 cycle) and *ROGF* (from −0.8 to 3.1 m/s) change dramatically in the scintillation level of S_4 ranging from 0.6 to 1.0. That means strong amplitude scintillation in low-latitude can result in more cycle-slips occurrences, thus significantly affecting GNSS measurements. The right two panels show that large fluctuations of ΔN_{WL} and *ROGF* values concentrate in the range of σ_φ from 5° to 30° for GPS, GLONASS, and BDS. It is clear that most large ΔN_{WL} and *ROGF* located in the area of σ_φ < 15° are caused by amplitude scintillation events. Noted that some large ΔN_{WL} and *ROGF* located in the area of 15° < σ_φ < 30° are also caused by strong amplitude scintillations (0.6 < S_4 <1.0) instead of weaker phase scintillations (15° < σ_φ < 30°). The analysis of easier occurrence of cycle-slips under strong amplitude scintillations in low-latitude will be shown in the section 3.2. In Fig. 4, some large ΔN_{WL} and *ROGF* can be seen under the threshold of S_4 = 0.2, which means that these cycle-slips should not be caused by scintillations. Except for ionospheric scintillation, cycle-slips can also be caused by obstruction of satellite signal and the failure in receiver software (Hofmann-Wellenhof et al., 2008).

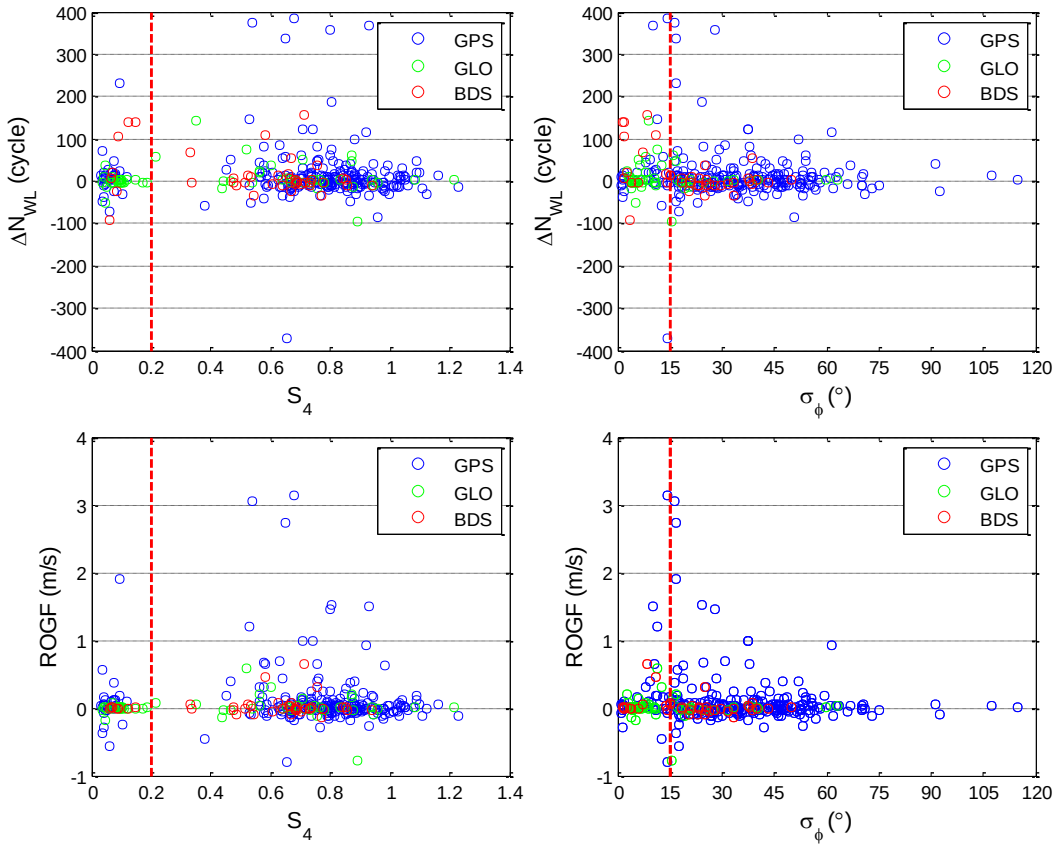

Fig. 4 Distribution of ΔN_{WL} and *ROGF* (during cycle-slip occurrence) against S_4 (amplitude scintillation) and σ_φ (phase scintillation) for GPS, GLONASS, and BDS satellites data collected at Sha Tin station in Hong Kong from 6 October 2015 to 31 December 2016

The hourly statistics of scintillation and cycle-slips can help identify the most likely period within a day when scintillation events and cycle-slips may occur. Based on the data collected at Sha Tin station from 6 October 2015 to 31 December 2016, the occurrence probability of scintillation events and cycle-slips as a

function of LT for GPS, GLONASS, and BDS is shown in Fig. 5. The hourly occurrence probability of scintillation events (or cycle-slips) is defined as the ratio between the number of scintillation events (or cycle-slips) in one hour and the total number of all scintillations events (or cycle-slips) in 24 hours from 6 October 2015 to 31 December 2016. As seen in the top panels of Fig. 5, the occurrence of ionospheric scintillation at Sha Tin station is characterized by a nighttime phenomenon, which occurs frequently from 20:00 LT to 0:00 LT. During this period of time, the occurrence probabilities of scintillation events are 85.5%, 67.8%, and 90.7% for GPS, GLONASS, and BDS, respectively. The number of scintillation events in the time period from 18:00 LT to 6:00 LT is presented in Table 3. The nighttime scintillation activity is mainly caused by generation of post sunset electron density irregularities in the equatorial ionosphere (Seif et al., 2012; Spogli et al., 2013).

As shown in the bottom panels of Fig. 5, most of the cycle-slips are detected during the time from 20:00 LT to 00:00 LT. A clear peak appeared at around 20:00 LT. The statistical results show that the cycle-slips detected during 20:00–0:00 LT account for 78.7%, 66.1%, and 87.8% for GPS, GLONASS, and BDS, respectively. As analyzed before, most scintillation events are also found in this time period, suggesting that cycle-slips occurring in 20:00–00:00 LT are mainly caused by ionospheric scintillations. This is consistent with the reports by other researchers (Oksavik et al., 2015; Zhang et al., 2010). The detailed statistics of cycle-slips in the presence of scintillation events for different GNSS systems are shown in Table 3. During 18:00–6:00 LT, the averaged ratio value, between the number of cycle-slips and scintillation events, for GPS, GLONASS, and BDS are 0.02, 0.03, and 0.07, respectively. It is obvious that the ratio changes substantially between different GNSS constellations.

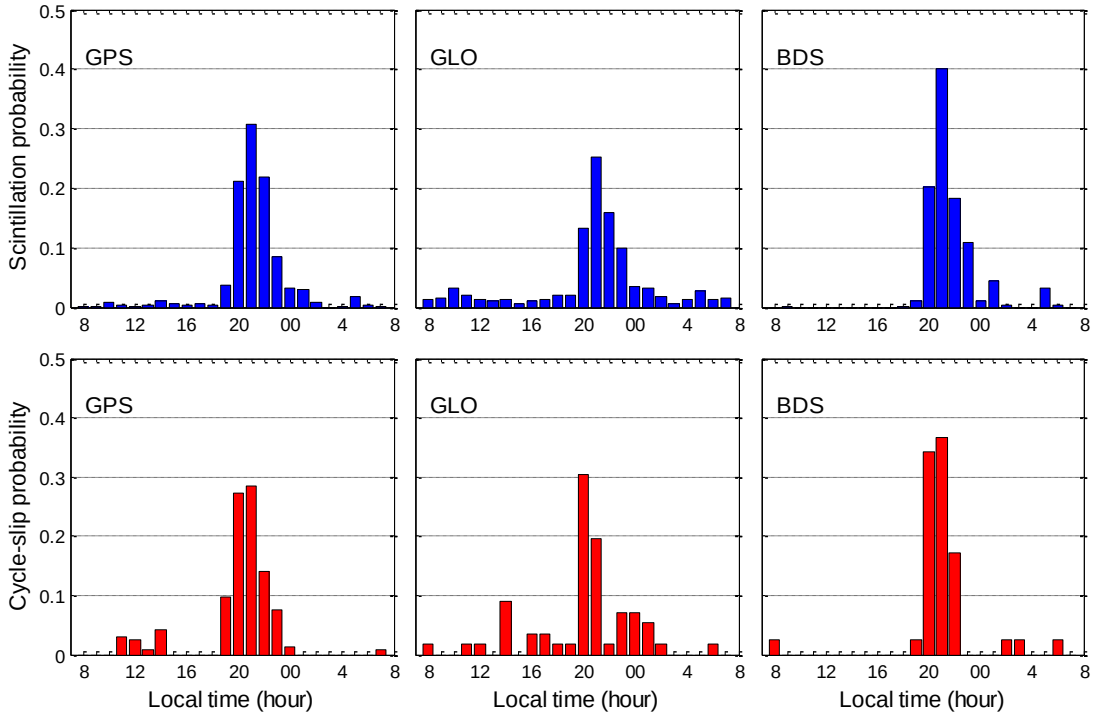

Fig. 5 Hourly occurrence probability of scintillation events and cycle-slips for GPS, GLONASS, and BDS satellites data collected at Sha Tin station from 6 October 2015 to 31 December 2016

Table 3 Statistical summary of scintillation event and cycle-slip occurring in each hour from 18:00 LT to 6:00 LT for different GNSS satellites observed from 6 October 2015 to 31 December 2016

	18:00	19:00	20:00	21:00	22:00	23:00	0:00	1:00	2:00	3:00	4:00	5:00	6:00

GPS	Scintillation	17	150	878	1279	907	351	136	124	31	0	1	73	14
	Cycle-slip	0	23	64	67	33	18	3	0	0	0	0	0	0
GLO	Scintillation	49	47	302	573	362	227	79	74	43	14	31	62	28
	Cycle-slip	1	1	17	11	1	4	4	3	1	0	0	0	1
BDS	Scintillation	1	11	215	425	195	115	12	46	3	0	0	33	3
	Cycle-slip	0	1	14	15	7	0	0	0	1	1	0	0	1

3.2. Daily distribution of scintillations and cycle-slips

The daily distribution of amplitude scintillation events and phase scintillation events from 6 October 2015 to 31 December 2016 is shown in Fig. 6. The vertical dashed lines separate the data period of 2015 (left) and 2016 (right). The equinoctial (March–April, September–October) months are highlighted in gray. The total numbers of amplitude and phase scintillation events occurred in multi-GNSS systems i.e. GPS, GLONASS, BDS, and Galileo are also presented in Fig. 6. Fig. 6 shows that scintillations often occur around the equinox months, which is consistent with others' work (Huang et al., 2014; Liu et al., 2015). The seasonal variation of scintillation may be associated with solar activity (Deng et al., 2013), but seasonal dependence of pre-reversal enhancement (PRE) of vertical drift of plasma bubble should play a dominant role for that (Fejer et al., 1995; Ji et al., 2013a). From Fig. 6, it also can be found that the total number of amplitude scintillations is much larger than that of phase scintillations. This is consistent with most previous studies, which concluded that amplitude scintillations are more frequent and intense than phase scintillations in low-latitude region like Hong Kong (Xu et al., 2012; Yang and Liu, 2015). From DOY 279 to 321 in 2015, under a relatively high solar activity with the average $F10.7$ as 106, one scintillation of strong intensity occurred. The detailed daily distribution of scintillations and cycle-slips occurring from DOY 279 to 321 in 2015 is shown next.

Fig. 7 shows the daily statistics of scintillation events and cycle-slips based on three GNSS satellites data collected from 6 October 2015 (DOY 279) to 17 November 2015 (DOY 321). The blue bar represents scintillation event, and the red bar stands for cycle-slip. In Fig. 7, the total numbers of scintillation events observed by GPS, GLONASS, and BDS satellites are 2670, 1114, and 978 respectively from DOY 279 to 321 As a result of strong ionospheric scintillation influence, cycle-slips with a total number of 127, 28, and 37 are detected in the same time period in the GPS, GLONASS, and BDS data, respectively.

However, no cycle-slip occurrence is detected in some nights, e.g., DOY 279, 283, 288, and 300 in 2015 although scintillation events are observed in these days in Fig. 7, especially in the case of DOY 279 when scintillations are detected in the GNSS signals of all the three GNSS systems. Seo et al. (2009) and Zhang et al. (2010) suggest that low scintillation level ($0.2 < S_4 \leq 0.6$) possibly leads to GNSS signal fading instead of loss of lock. In the same scintillation level, whether the cycle-slip will occur or not is also related to the receiver tracking model (de Oliveira Moraes et al., 2014). Fig. 8 gives an example to show this phenomenon using the BDS satellite C01 dataset collected on DOY 279. The black line in the third panel represents the threshold of scintillation occurrence. As we can see from Fig. 8, six amplitude scintillation events are observed at epochs 21:46:00, 22:05:00, 22:08:00, 22:30:00, 22:31:00, and 22:37:00 LT, respectively, but the curve of N_{WL} and *ROGF* fluctuate only slightly during 21:45 to 22:40 LT, below the threshold of cycle-slip occurrence.

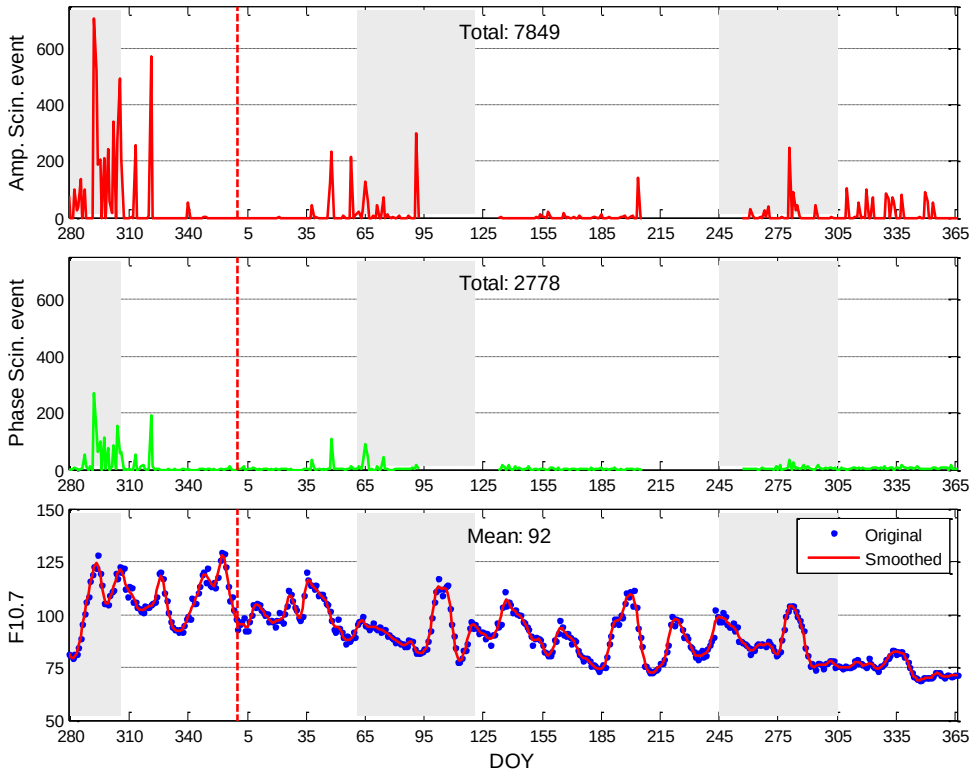

Fig. 6 Variations of amplitude scintillation event number and phase scintillation event number under corresponding solar activity from 6 October 2015 (DOY 279) to 31 December 2016 (DOY 366)

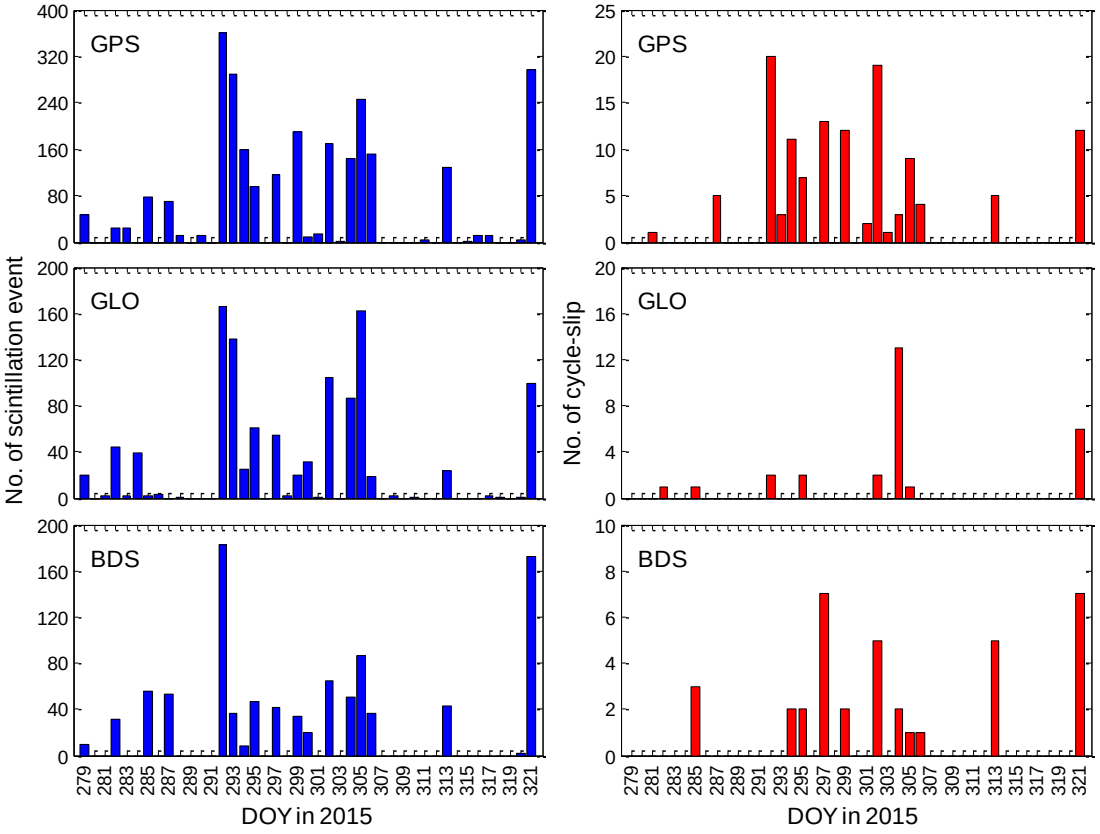

Fig. 7 Daily distribution of the number of scintillation events and cycle-slips using GPS, GLONASS, and BDS satellites data collected at Sha Tin station in Hong Kong from 6 October 2015 (DOY 279) to 17 November 2015 (DOY 321)

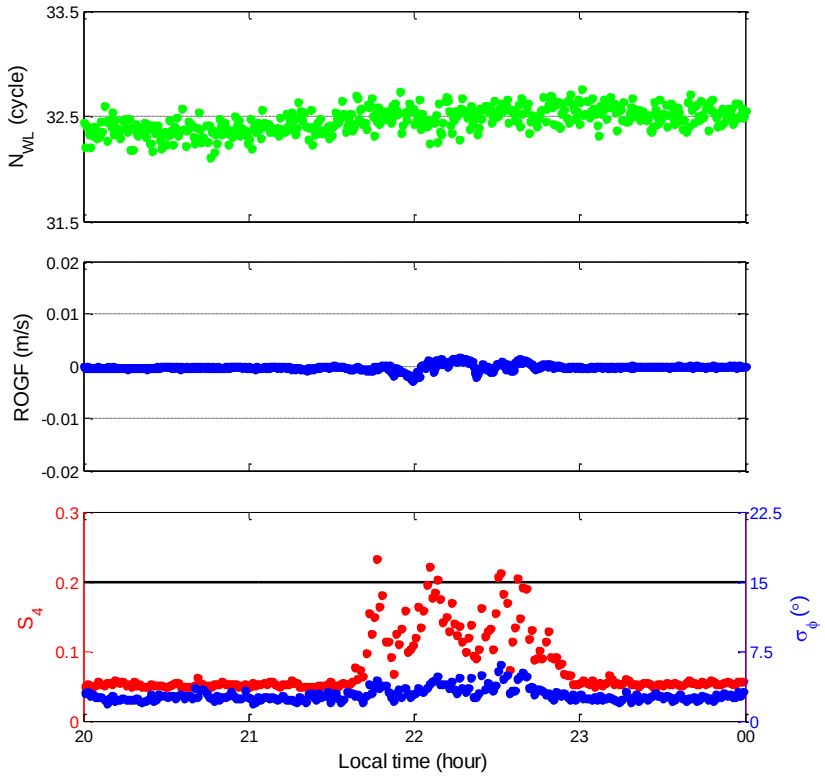

Fig. 8 An example of no cycle-slip occurrence when scintillation events are observed using the BDS satellite C01 dataset collected on DOY 279 in 2015 (6 October 2015)

To further investigate the correlation between the occurrence of cycle-slip and ionospheric scintillation level, the daily statistics of the number of scintillation events and cycle-slips at two S_4 levels, i.e. $0.2 < S_4 \leq 0.6$ and $S_4 > 0.6$ are presented in Fig. 9. The Multi-GNSS data collected from DOY 279 to DOY 321 in 2015 are chosen since most scintillation events and cycle-slips occurred in this period of time (see Fig. 7). There are 4774 amplitude scintillation events, 1496 phase scintillation events, and 4881 all scintillation events occurring in multi-GNSS systems i.e. GPS, GLONASS, BDS, and Galileo. Noted that the total 4881 scintillation events include 1389 amplitude and phase scintillation events occurring at the same time, i.e., (4774+1496−1389). Considering the smaller number of events, phase scintillation is not discussed next. Noted that the average sunspot number and $F10.7$ for this period are 67 and 106, respectively, which is a moderate solar flux condition. In this study, we assume that the cycle-slip is resulted from scintillation if both cycle-slip and scintillation are detected in a satellite measurement. From Fig. 9, it can be clearly seen that more scintillation events occurred in weak scintillation level of $0.2 < S_4 \leq 0.6$ compared with those occurred in strong level of $S_4 > 0.6$. However, the number of cycle-slips caused by strong scintillation events is much higher than that of weak scintillation events regardless of GPS, GLONASS, or BDS. Our results showed that weak scintillation events, observed in GPS, GLONASS, and BDS, account for 79.0%, 88.1%, and 84.5%, and they led to occurrence of cycle-slips of 12.1%, 40.7%, and 27.8% in the three GNSS systems. The strong scintillation events only account for 21.0% (GPS), 11.9% (GLONASS), and 15.5% (BDS), but they caused occurrence of cycle-slip of 87.9%, 59.3%, and 72.2% in the three GNSS systems, respectively. In other words, each 1000 strong scintillation events ($S_4 > 0.6$) can result in 200, 124, and 171 cycle-slip occurrences in GPS, GLONASS, and BDS respectively, while each 1000 weak scintillation events ($0.2 < S_4 \leqslant 0.6$) just result in 7, 12, and 12 cycle-slip occurrences in the three systems.

Detailed daily scintillation and cycle-slip occurrence probability under five levels of amplitude scintillation are shown in Fig. 10. The five S_4 levels are $0.2 < S_4 \leq 0.4$, $0.4 < S_4 \leq 0.6$, $0.6 < S_4 \leq 0.8$, $0.8 < S_4 \leq 1.0$ and $S_4 > 1.0$, respectively. Like Fig. 9, the Multi-GNSS data collected from DOY 279 to DOY 321 in 2015 are chosen in this plot. From the left panels of Fig. 10, we can see that the larger the S_4 levels, the smaller occurrence probability of amplitude scintillation events for GPS, GLONASS, and BDS. The left panels also show that very few scintillation events occur in the strong level with $S_4 > 1.0$. Since all the 43 datasets are under moderate solar flux conditions, strong scintillations occurrence are not frequent during this conditions (de Oliveira Moraes et al., 2012; Jiao and Morton, 2015). The right panels of Fig. 10 show that the scintillation events at the $0.6 < S_4 \leq 0.8$ and $0.8 < S_4 \leq 1.0$ levels contribute more cycle-slip occurrences (75.4%). In addition, few cycle-slips result from scintillation events at $0.2 < S_4 \leq 0.4$ level for Multi-GNSS although more amplitude scintillation events occur in this level.

Another information worth mentioning is the time between cycle-slips for GPS, GLONASS, and BDS constellations. From DOY 279 to DOY 321 in 2015, statistical results suggest that the maxima time between two cycle-slips is 20.5, 18.5, and 51.5 minutes for GPS, GLONASS, and BDS respectively. The average time between cycle-slips is 4.6, 5.2, and 15.4 minutes for the GPS, GLONASS, and BDS, respectively.

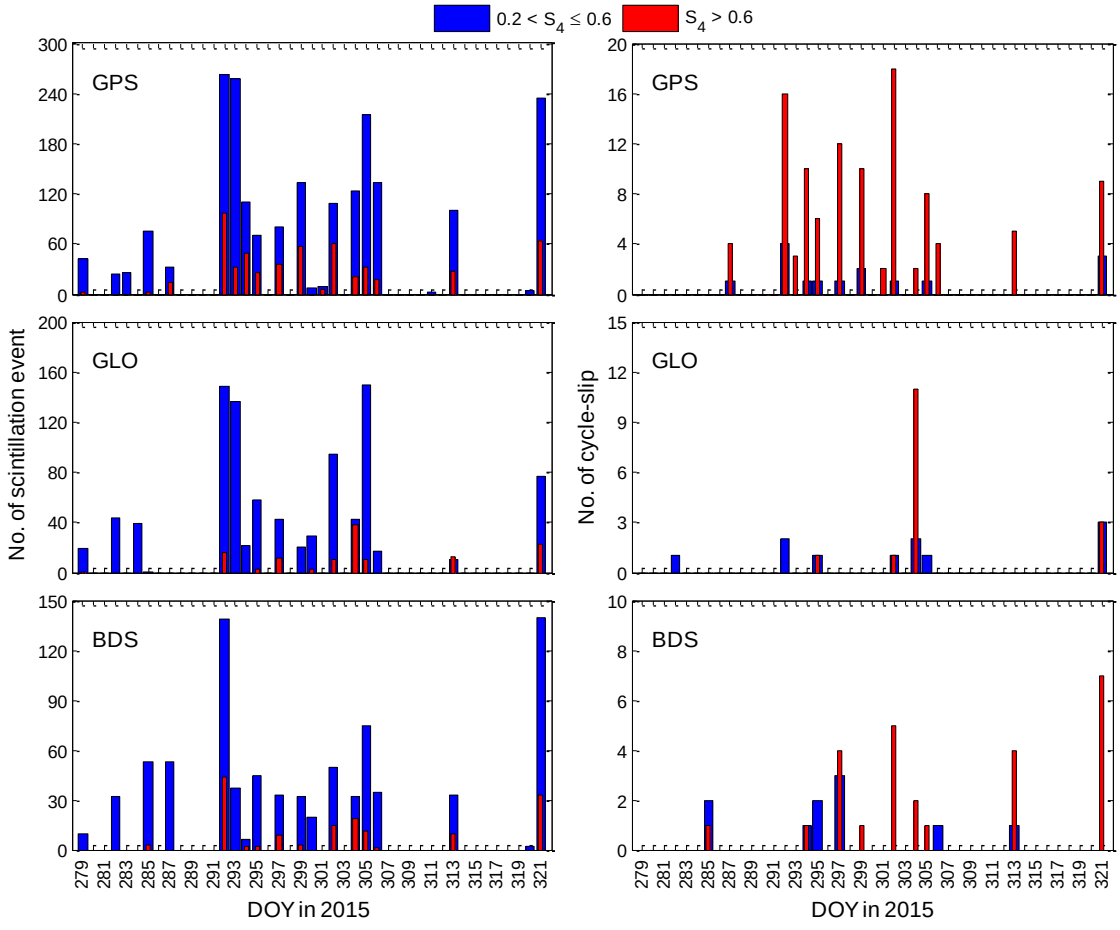

Fig. 9 Statistics of the number of scintillation events and cycle-slips at two S_4 levels, i.e. $0.2 < S_4 \leq 0.6$ and $S_4 > 0.6$, using Multi-GNSS data collected at Sha Tin station from 6 October 2015 (DOY 279) to 17 November 2015 (DOY 321)

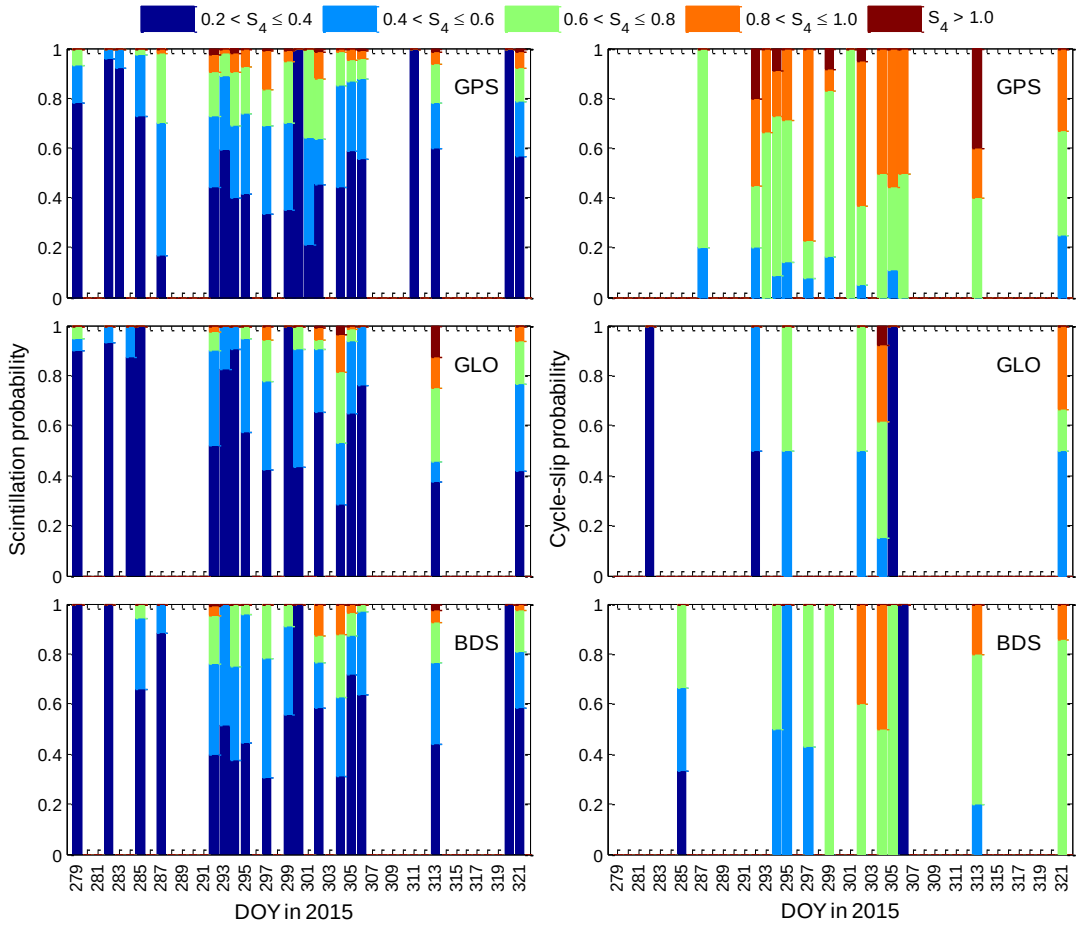

Fig. 10 Scintillation and cycle-slip occurrence probability at five S_4 levels, i.e. $0.2 < S_4 \leq 0.4$, $0.4 < S_4 \leq 0.6$, $0.6 < S_4 \leq 0.8$, $0.8 < S_4 \leq 1.0$ and $S_4 > 1.0$, using Multi-GNSS data collected at Sha Tin station from 6 October 2015 (DOY 279) to 17 November 2015 (DOY 321)

3.3. Spatial distribution of scintillations and cycle-slips

Fig. 11 depicts the spatial distribution of scintillations and cycle-slips at five S_4 levels, i.e. $0.2 < S_4 \leq 0.4$, $0.4 < S_4 \leq 0.6$, $0.6 < S_4 \leq 0.8$, $0.8 < S_4 \leq 1.0$ and $S_4 > 1.0$, using all GPS, GLONASS, and BDS data collected at Sha Tin station from 6 October 2015 (DOY 279) to 31 December 2016 (DOY 366). The cut-off elevation angle is 30°. From the left panels of Fig. 11, the majority of scintillations occur in the southern sky of Sha Tin station. Recent observations by Liu et al. (2015) also show that an occurrence peak of scintillations is located at the southern sky of Sanya in China. The main reason is related to the moderate solar activity strength from 6 October 2015 (DOY 279) to 31 December 2016 (DOY 366) (see Fig. 6). In a stronger solar flux condition the irregularities would evolve further north and as a consequence the occurrences in this sector would be increased (de Oliveira Moraes et al., 2012; Liu et al., 2015). Moreover, it is clear that the irregularities rise from the equatorial region and that Sha Tin station is located at the north of equator region, so the south sector of Sha Tin station would be the most susceptible region. Fig. 11 also shows more scintillations during this period time are level 1 scintillations. The level 1 scintillations located in the southern sky account for 45.6%, 52.7%, and 50.3% for GPS, GLONASS, and BDS, respectively. Compared to scintillations, the number of cycle-slips is much fewer. The main reason is that most low level (< 3) scintillations do not lead to the occurrence of cycle-slip (see Fig. 4 and Fig. 8). From Fig. 11, we can see that near all of cycle-slips are detected in the south area, where the scintillation events occur more frequently. Noted that most cycle-slip occurrences are associated with the level 3 and 4 scintillations, which is consistent with the observation from Fig. 10.

We find that most scintillations and cycle-slips observed in the elevation zone from 30° to 60°. In this elevation zone, 85.3%, 77.0%, and 69.9% scintillation events and 94.1%, 75.8%, 86.1% cycle-slips occur for GPS, GLONASS, and BDS, respectively. Because a cut-off elevation of 30° has been used in this study, the multipath effect on scintillation events can basically be neglected. As we know, satellite signals with a higher elevation has a shorter propagation path through ionosphere area than lower elevation signals (Mohino, 2008). Therefore, the probability of scintillation events in higher elevation is smaller than that in lower elevation on the whole. Moreover, the ionospheric irregularities (e.g., plasma bubble) would be depleted along with the increase of satellite elevation angle (Deng et al., 2013; Huang et al., 2014).

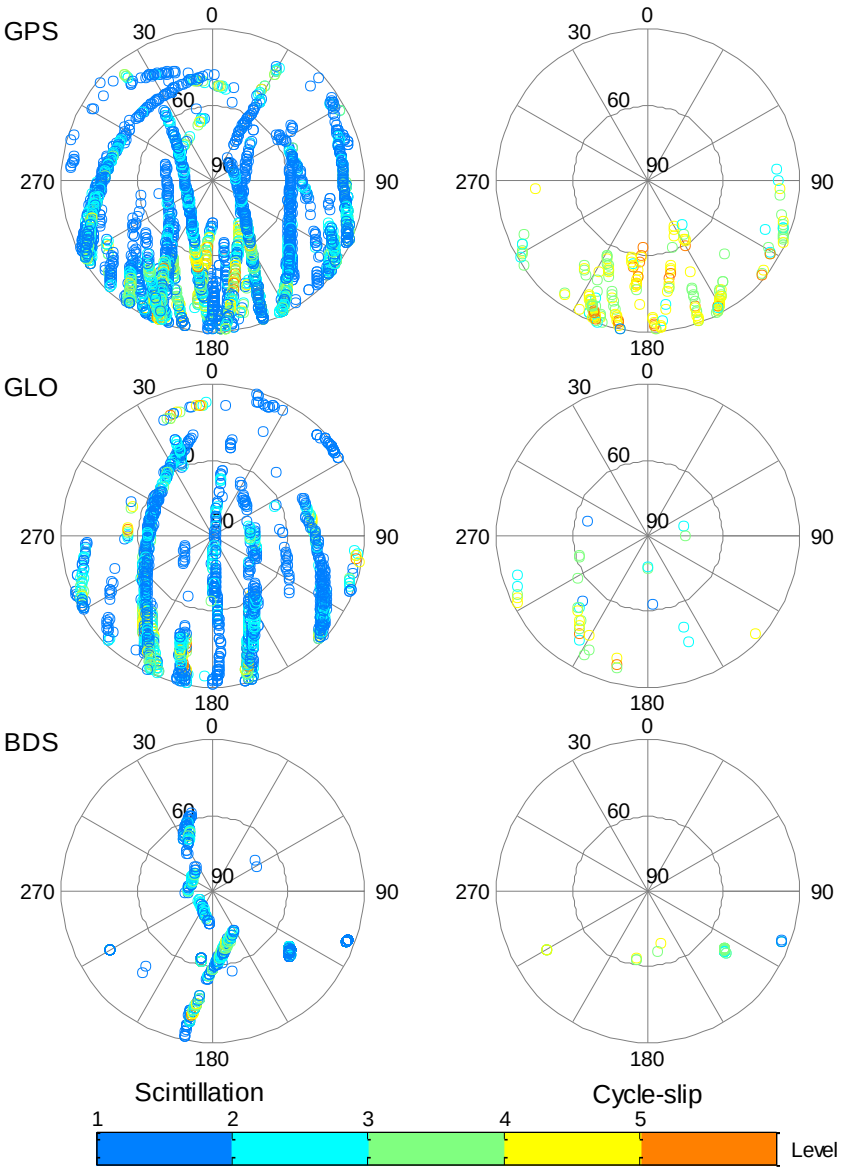

Fig. 11 Spatial distribution of scintillations and cycle-slips at five S_4 levels, i.e. $0.2 < S_4 \leq 0.4$, $0.4 < S_4 \leq 0.6$, $0.6 < S_4 \leq 0.8$, $0.8 < S_4 \leq 1.0$ and $S_4 > 1.0$, using Multi-GNSS data collected at Sha Tin station from 6 October 2015 (DOY 279) to 31 December 2016 (DOY 366)

4. Conclusions

This study investigates the characteristics of Multi-GNSS ionospheric scintillation and cycle-slip occurrence by analyzing the scintillation data and Multi-GNSS measurements. A total of 363 days of data

collected by a newly installed GNSS scintillation monitoring receiver located at Sha Tin of Hong Kong for the time period from 6 October 2015 to 31 December 2016 has been analyzed. This period of time was under a moderate solar activity condition with the average sunspot number and $F10.7$ are 44 and 92, respectively. In the process of cycle-slip detection, a ROGF combination is proposed to take the size of time gap between two data arcs into account since the loss of lock occurs frequently in GNSS measurements in the presence of ionospheric scintillation conditions.

The hourly occurrence probability indicates that 85.5%, 67.8%, and 90.7% scintillations and 78.7%, 66.1%, and 87.8% cycle-slips are observed during 20:00 LT to 00:00 LT at GPS, GLONASS, and BDS measurements, respectively. In strong scintillation ($S_4 > 0.6$) conditions, the time series of WL ambiguity N_{WL} and $ROGF$ vary significantly. The range of N_{WL} and $ROGF$ can reach more than 50 cycles and 0.1 m/s, respectively. However, the weak scintillations ($0.2 < S_4 \leq 0.6$) possibly lead to GNSS signal fading instead of cycle-slip. Under the moderate solar condition (mean $F10.7 = 106$) from 6 October to 17 November of 2015, the daily statistics results show that each 1000 strong scintillation events ($S_4 > 0.6$) can result in 200, 124, and 171 cycle-slip occurrences in GPS, GLONASS, and BDS, respectively, whereas each 1000 weak scintillation events ($0.2 < S_4 \leq 0.6$) just result in about 7, 12, and 12 cycle-slip occurrences in the three systems. A detailed daily scintillation and cycle-slip occurrence probability show that 75.4% cycle-slips occur in the scintillation levels of $0.6 < S_4 \leq 0.8$ and $0.8 < S_4 \leq 1.0$. The spatial distribution results indicate that most scintillations and near all of cycle-slips are observed in the southern sector, mainly associated with the moderate solar condition (mean $F10.7 = 92$) and intense irregularities from equatorial region. Meanwhile, majority of them occur in the elevation zone from 30° to 60° since they are influenced more by ionospheric irregularity effect. The spatial distribution results also show that cycle-slip occurrences are mainly caused by the level 3 and 4 scintillations. It should be mentioned that the hourly, daily, and spatial distribution results of Galileo scintillations and cycle-slips are also taken into account by our work, but they are not noticeable compared to other three systems due to the insufficient Galileo satellites during this period of time.

This study can contribute to GNSS users of the equatorial anomaly region to carefully use GNSS measurements influenced by the strong ionospheric scintillation. A relatively flexible threshold of cycle-slip detection may help to minimize unnecessary ambiguity initialization in GNSS PPP; and a lower weight for measurements polluted by scintillation may improve positioning performance in GNSS RTK and PPP application.

Acknowledgments

The supports from the National Key Research and Development Program of China (2016YFB0501802) are gratefully acknowledged. The authors Xiaomin Luo, Zhizhao Liu, and Biyan Chen would like to acknowledge the supports from the Hong Kong Research Grants Council (RGC) (project PolyU 5325/12E (F-PP0F)), the National Natural Science Foundation of China (project No. 41274039), and the Hong Kong Polytechnic University (project G-YBM3). The authors are also grateful to the NASA/GSFC Space Physics Data Facility's OMNIWeb service (https://omniweb.gsfc.nasa.gov) for providing sunspot number and solar flux index $F10.7$ data.

References

Aquino, M., Moore, T., Dodson, A., Waugh, S., Souter, J., Rodrigues, F.S., 2005. Implications of ionospheric scintillation for GNSS users in northern Europe. J. Navig. 58, 241–256. doi:10.1017/S0373463305003218

Banville, S., Langley, R.B., 2013. Mitigating the impact of ionospheric cycle slips in GNSS observations. J.

Geod. 87, 179–193. doi:10.1007/s00190-012-0604-1

Banville, S., Langley, R.B., Saito, S., Yoshihara, T., 2010. Handling cycle slips in GPS data during ionospheric plasma bubble events. Radio Sci. 45, 1–14. doi:10.1029/2010RS004415

Bernhardt, P.A., Siefring, C.L., Galysh, I.J., Rodilosso, T.F., Koch, D.E., MacDonald, T.L., Wilkens, M.R., Landis, G.P., 2006. Ionospheric applications of the scintillation and tomography receiver in space (CITRIS) mission when used with the DORIS radio beacon network. J. Geod. 80, 473–485. doi:10.1007/s00190-006-0064-6

Blewitt, G., 1990. An automatic editing algorithm for GPS data. Geophys. Res. Lett. 17, 199–202. doi:10.1029/GL017i003p00199

Briggs, B.H., Parkin, I.A., 1963. On the variation of radio star and satellite scintillations with zenith angle. J. Atmos. Terr. Phys. 25, 339–366. doi:10.1016/0021-9169(63)90150-8

Chen, W., Gao, S., Hu, C., Chen, Y., Ding, X., 2008. Effects of ionospheric disturbances on GPS observation in low latitude area. GPS Solut. 12, 33–41. doi:10.1007/s10291-007-0062-z

Crane, R.K., 1977. Ionospheric Scintillation. Proc. IEEE 65, 180–199. doi:10.1109/PROC.1977.10456

de Oliveira Moraes, A., Costa, E., Abdu, M.A., Rodrigues, F., de Paula, E.R., Oliveira, K., Perrella, W.J., 2017. The variability of low-latitude ionospheric amplitude and phase scintillation detected by a triple-Frequency GPS receiver. Radio Sci. doi:10.1002/2016RS006165

de Oliveira Moraes, A., Costa, E., de Paula, E.R., Perrella, W.J., Monico, J.F.G., 2014. Extended ionospheric amplitude scintillation model for GPS receivers. Radio Sci. 49, 315–329. doi:10.1002/2013RS005307

de Oliveira Moraes, A., da Silveira Rodrigues, F.S., Perrella, W.J., de Paula, E.R., 2012. Analysis of the characteristics of low-latitude GPS amplitude scintillation measured during solar maximum conditions and implications for receiver performance. Surv. Geophys. 33, 1107–1131. doi:10.1007/s10712-011-9161-z

Deng, B., Huang, J., Liu, W., Xu, J., Huang, L., 2013. GPS scintillation and TEC depletion near the northern crest of equatorial anomaly over South China. Adv. Sp. Res. 51, 356–365. doi:10.1016/j.asr.2012.09.008

Fejer, B.G., de Paula, E.R., Heelis, R.A., Hanson, W.B., 1995. Global equatorial ionospheric vertical plasma drifts measured by the AE-E satellite. J. Geophys. Res. 100, 5769–5776. doi:10.1029/94JA03240

Ge, M., Gendt, G., Rothacher, M., Shi, C., Liu, J., 2008. Resolution of GPS carrier-phase ambiguities in Precise Point Positioning (PPP) with daily observations. J. Geod. 82, 389–399. doi:10.1007/s00190-007-0187-4

Grejner-Brzezinska, D. A., Kashani, I., Wielgosz, P., Smith, D. A., Spencer, P.S.J., Robertson, D.S., Mader, G.L., 2007. Efficiency and reliability of ambiguity resolution in network-based real-time kinematic GPS. J. Surv. Eng. 133, 56–65. doi:10.1061/(ASCE)0733-9453(2007)133:2(56)

Gwal, A., Dubey, S., Wahi, R., Feliziani, A., 2006. Amplitude and phase scintillation study at Chiang Rai, Thailand. Adv. Sp. Res. 38, 2361–2365. doi:10.1016/j.asr.2006.02.057

Hofmann-Wellenhof, B., Lichtenegger, H., Wasle, E., 2007. GNSS-global navigation satellite systems: GPS, GLONASS, Galileo and more. Springer Science & Business Media

Huang, L., Wang, J., Jiang, Y., Chen, Z., Zhao, K., 2014. A study of GPS ionospheric scintillations observed at Shenzhen. Adv. Sp. Res. 54, 2208–2217. doi:10.1016/j.asr.2014.08.023

Ji, S., Chen, W., Wang, Z., Xu, Y., Weng, D., Wan, J., Fan, Y., Huang, B., Fan, S., Sun, G., Wang, H., Song, D., He, Y., 2013a. A study of occurrence characteristics of plasma bubbles over Hong Kong area. Adv. Sp. Res. 52, 1949–1958. doi:10.1016/j.asr.2013.08.026

Ji, S., Chen, W., Weng, D., Wang, Z., Ding, X., 2013b. A study on cycle slip detection and correction in case of ionospheric scintillation. Adv. Sp. Res. 51, 742–753. doi:10.1016/j.asr.2012.10.012

Jiao, Y., Morton, Y.T., 2015. Comparison of the effect of high-latitude and equatorial ionospheric scintillation on

GPS signals during the maximum of solar cycle 24. Radio Sci. 50, 886–903. doi:10.1002/2015RS005719

Jiao, Y., Morton, Y.T., Taylor, S., Pelgrum, W., 2013. Characterization of high-latitude ionospheric scintillation of GPS signals. Radio Sci. 48, 698–708. doi:10.1002/2013RS005259

Kil, H., Heelis, R.A., 1998. Equatorial density irregularity structures at intermediate scales and their temporal evolution. J. Geophys. Res. 103, 3969–3981. doi:10.1029/97JA03344

Li, G., Ning, B., Ren, Z., Hu, L., 2010. Statistics of GPS ionospheric scintillation and irregularities over polar regions at solar minimum. GPS Solut. 14, 331–341. doi:10.1007/s10291-009-0156-x

Liu, K., Li, G., Ning, B., Hu, L., Li, H., 2015. Statistical characteristics of low-latitude ionospheric scintillation over China. Adv. Sp. Res. 55, 1356–1365. doi:10.1016/j.asr.2014.12.001

Liu, Z., 2011. A new automated cycle slip detection and repair method for a single dual-frequency GPS receiver. J. Geod. 85, 171–183. doi:10.1007/s00190-010-0426-y

Meggs, R.W., Mitchell, C.N., Honary, F., 2008. GPS scintillation over the European Arctic during the November 2004 storms. GPS Solut. 12, 281–287. doi:10.1007/s10291-008-0090-3

Milan, S.E., Basu, S., Yeoman, T.K., Sheehan, R.E., 2005. A comparison of satellite scintillation measurements with HF radar backscatter characteristics. Ann. Geophys. 23, 3451–3455. doi:10.5194/angeo-23-3451-2005

Mohino, E., 2008. Understanding the role of the ionospheric delay in single-point single-epoch GPS coordinates. J. Geod. 82, 31–45. doi:10.1007/s00190-007-0155-z

Moreno, B., Radicella, S., de Lacy, M.C., Herraiz, M., Rodriguez-Caderot, G., 2011. On the effects of the ionospheric disturbances on precise point positioning at equatorial latitudes. GPS Solut. 15, 381–390. doi:10.1007/s10291-010-0197-1

Oksavik, K., Meeren, C. van der, Lorentzen, D.A., Baddeley, L.J., Moen, J., 2015. Scintillation and loss of signal lock from poleward moving auroral forms in the cusp ionosphere. J. Geophys. Res. Sp. Phys. 120, 9161–9175. doi:10.1002/2013JA019381

Olwendo, O.J., Baki, P., Cilliers, P.J., Doherty, P., Radicella, S., 2016. Low latitude ionospheric scintillation and zonal plasma irregularity drifts climatology around the equatorial anomaly crest over Kenya. J. Atmos. Solar-Terrestrial Phys. 138–139, 9–22. doi:10.1016/j.jastp.2015.12.002

Prikryl, P., Ghoddousi-Fard, R., Kunduri, B.S.R., Thomas, E.G., Coster, A.J., Jayachandran, P.T., Spanswick, E., Danskin, D.W., 2013. GPS phase scintillation and proxy index at high latitudes during a moderate geomagnetic storm. Ann. Geophys. 31, 805–816. doi:10.5194/angeo-31-805-2013

Prikryl, P., Jayachandran, P., Mushini, S.C., Richardson, I.G., 2014. High-latitude GPS phase scintillation and cycle slips during high-speed solar wind streams and interplanetary coronal mass ejections: a superposed epoch analysis. Earth, Planets Sp. 66, 62. doi:10.1186/1880-5981-66-62

Prikryl, P., Jayachandran, P.T., Mushini, S.C., Pokhotelov, D., MacDougall, J.W., Donovan, E., Spanswick, E., St.-Maurice, J.P., 2010. GPS TEC, scintillation and cycle slips observed at high latitudes during solar minimum. Ann. Geophys. 28, 1307–1316. doi:10.5194/angeo-28-1307-2010

Seif, A., Abdullah, M., Hasbi, A. M., Zou, Y., 2012. Investigation of ionospheric scintillation at UKM station, Malaysia during low solar activity. Acta Astronaut. 81, 92–101. doi:http://dx.doi.org/10.1016/j.actaastro.2012.06.024

Seo, J., Walter, T., Chiou, T.Y., Enge, P., 2009. Characteristics of deep GPS signal fading due to ionospheric scintillation for aviation receiver design. Radio Sci. 44, 1–10. doi:10.1029/2008RS004077

Skone, S., Man, F., Ghafoori, F., Tiwari, R., 2008. Investigation of scintillation characteristics for high latitude phenomena, in: 21st International Technical Meeting of the Satellite Division of the Institute of Navigation, ION GNSS 2008. Inst. of Navig., Savanna, GA, pp. 2425–2434

Spogli, L., Alfonsi, L., Romano, V., De Franceschi, G., Joao Francisco, G.M., Hirokazu Shimabukuro, M., Bougard, B., Aquino, M., 2013. Assessing the GNSS scintillation climate over Brazil under increasing solar activity. J. Atmos. Solar-Terrestrial Phys. 105–106, 199–206. doi:10.1016/j.jastp.2013.10.003

Sreeja, V., Aquino, M., Elmas, Z.G., 2011. Impact of ionospheric scintillation on GNSS receiver tracking performance over Latin America: Introducing the concept of tracking jitter variance maps. Sp. Weather 9. doi:10.1029/2011SW000707

Van Dierendonck, A.J., Klobuchar, J., Hua, Q., 1993. Ionospheric scintillation monitoring using commercial single frequency C/A code receivers, in: Proceedings of the 6th International Technical Meeting of the Satellite Division of The Institute of Navigation, ION GPS 1993. Inst. of Navig., Salt Lake City, Utah, pp. 1333–1342

Weber, E.J., Buchau, J., Moore, J.G., Sharber, J.R., Livingston, R.C., Winningham, J.D., Reinisch, B.W., 1984. F layer ionization patches in the polar cap. J. Geophys. Res. Sp. Phys. 89, 1683–1694. doi:10.1029/JA089iA03p01683

Xu, R., Liu, Z., Li, M., Morton, Y., Chen, W., 2012. An analysis of low-latitude ionospheric scintillation and its effects on precise point positioning. J. Glob. Position. Syst. 11, 22–32. doi:10.5081/jgps.11.1.22

Yang, Z., Liu, Z., 2016. Correlation between ROTI and Ionospheric Scintillation Indices using Hong Kong low-latitude GPS data. GPS Solut. 20, 815–824. doi:10.1007/s10291-015-0492-y

Zhang, D., Xiao, Z., Feng, M., Hao, Y., Shi, L., Yang, G., Suo, Y., 2010. Temporal dependence of GPS cycle slip related to ionospheric irregularities over China low-latitude region. Sp. Weather 8, 1–10. doi:10.1029/2008SW000438

Zhang, X., Guo, F., Zhou, P., 2014. Improved precise point positioning in the presence of ionospheric scintillation. GPS Solut. 18, 51–60. doi:10.1007/s10291-012-0309-1